ROTATIONAL MICRO-MOTION MODULATED JAMMING FOR COUNTERING ISAR BASED ON INTERMITTENT SAMPLING REPEATER

Xiaoyi Pan[*], Wei Wang, Dejun Feng, Jing Huang, Qixiang Fu, and Guoyu Wang

School of Electronic Science and Engineering, National University of Defense Technology, Changsha 410073, China

Abstract—The intermittent sampling repeater jamming (ISRJ) can only produce fake point scatterers in the down-range, while the time-varying frequency induced by rotational micro-motion dynamics blurs the image in the cross-range. This paper focuses on the combination of the above two methods to counter the inverse synthetic aperture radar (ISAR). Based on the signal models of coherent ISAR signal processing, principles of the jamming are derived. The key jamming parameters and the selection criteria are determined by two steps. Finally, the validity of the proposed algorithm is demonstrated using the numeric simulations and simulations based on the measured data.

1. INTRODUCTION

The inverse synthetic aperture radar (ISAR) collects modulated pulses and coherently processes them to reconstruct a two-dimensional (2-D) intensity image of moving targets (such as aircraft and ships) [1–3]. ISAR imaging plays an important role in many military applications such as target classification, recognition and identification [4]. Surveillance systems such as US ALCOR radar [5], the AN/APS-137B(V) radar [6] and the ground based radar (GBR) [7] possess the capability of detecting, classifying and tracking by using the ISAR imaging mode. ISAR image, characterized by high resolution along both the range and cross-range directions, can also be used to launch weapon systems [6]. The need for countering wideband ISAR imaging radars remains a high priority in electronic warfare [8, 9].

In most of the conventional work on the inverse synthetic aperture radar (ISAR) imaging, the target is assumed to have rigid-body motion. Actually, non-rigid-body targets can often be found in real-world situations, such as the rotating rotor blades of a helicopter, the scanning antenna of a ship and the wheel of a ground vehicle [10–12]. These mechanical rotations or vibrations are referred as micro-motion dynamics. Micro-motion dynamics of an object or structures on the object may introduce additional time-varying frequency modulations on the radar echoes which are called micro-Doppler (m-D) effect [13, 14]. On the one hand, the ISAR image may be contaminated due to the interference from the additional time-varying m-D modulations when the backscattering of the micro-motion part is emphatic enough [15–17]. On the other hand, micro-Doppler features can be regarded as a unique signature of an object with movements, providing additional information for the classification, recognition, and identification of the object. Some methods for separation of the m-D effect or extract the m-D features from the radar echoes are proposed [10, 18–21]. Thus, the micro-motion dynamics can be used in the countermeasures of ISAR which may decrease the readability of radar images or make the separation and extraction of m-D signatures difficult and spurious.

A jamming method based on the rotating angular reflector is presented in [22]. With the characteristic of rotation, the frequency modulated radar echoes along azimuth lead to smeared imaging in ISAR. But it can only blur the image in the cross-range and the achieved barrage jamming along the down-range needs a reflector array as the author has pointed out. Actually, the jamming method based on the rotating angular reflector is a passive jamming technique and the reflector array may be difficult to set up especially in some aerospace targets, such as aircraft and ballistic targets on which space is limited. The digital radio frequency memory (DRFM) is widely used in radar active coherent jamming [6, 23–26]. With the capability of high speed sampling, DRFM reduces production costs and achieves a wide bandwidth. Associated with the micro-motion dynamics, Zhu et al. [27, 28] put forward the synthesizing equivalent micro-motion point jamming (SEMPJ) to ISAR based on DRFM. First, the intercepted ISAR signal samples are modulated by sinusoidal increments in the slow time. Second, all the samples are retransmitted to the radar. It can produce time-varying Doppler frequency modulations in the cross-range after ISAR imaging. Multiple point-scatterers will be induced in the down-range by utilizing the time-delay or frequency-shifted processing. One obvious problem of the SEMPJ is that the jamming signal retransmitted to the radar

usually is delayed at least one pulse duration compared with the target echoes. Based on the delay time, false targets may be identified by the radar easily [29]. High isolation of the two receive-transmit antennas is another problem in the coherent jamming. Based on a receive-transmit time-sharing antenna, the intermittent sampling repeater jamming (ISRJ) was proposed and developed [30]. It samples the arrived ISAR chirp signals intermittently for a constant time that is less than the pulse duration and then turns on the transmitter to retransmits all the samples immediately to the radar. Then the transmitter is turned off and the receiver is turned on to go on sampling the remainder signal. The steps of switching between the receiver and transmitter are alternated until the whole pulse has been sampled and retransmitted. Since the intermittent sampling is done in the fast time, false point scatterers will be introduced only in the down-range where each point spread function (PSF) is a scaled sinc function. As ISAR is a method of reconstructing a 2-D intensity image of a target, a jamming method that can contaminate the ISAR image in both the down-range and the cross-range is needed.

Based on the combination of the intermittent sampling in the fast time and the m-D modulation in the slow time, an ISAR jamming method is presented in this paper, which can introduce a smeared 2-D ISAR image. The remainder of this paper is organized as follows. The principles and the imaging results of jamming are derived in Section 2. Section 3 is dedicated to the analysis of important parameters and their selection criteria. In Section 4, numerical simulation results are presented and analyzed. In Section 5, the jamming simulations based on the measured data are discussed. Finally, in Section 6, some conclusions and perspectives are presented.

2. PRINCIPLES OF THE JAMMING

2.1. Intermittent Sampling in the Fast Time

Once the jammer receives the ISAR transmitted signal, it samples the pulse intermittently in the fast time and transmits all the samples immediately to the radar. Assume that the intermittent sampling
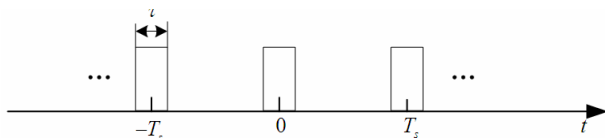
Figure 1. Intermittent sampling pulse series.

function noted as $p(t)$ is a rectangular envelope pulse train with pulse duration $\tau$and pulse repetition interval (PRI) T_s, as Fig. 1 illustrates, is defined as [30]

$$p(t) = \text{rect}\left(\frac{t}{\tau}\right) * \sum_{n=-\infty}^{+\infty} \delta(t - nT_s) \tag{1}$$

Consider an ISAR that transmits a linear frequency modulated pulse where the frequency is swept upwards cross the pulse. The waveform of the transmitted signal in the fast time and the slow time domain can be expressed as

$$s_0\left(\hat{t}, t_m\right) = \text{rect}\left(\frac{\hat{t}}{T_P}\right) e^{j2\pi\left(f_0 t + \frac{1}{2}k\hat{t}^2\right)} \tag{2}$$

where

$$\text{rect}\left(\frac{\hat{t}}{T_P}\right) = \begin{cases} 1 & \text{for } \left|\frac{\hat{t}}{T_P}\right| < \frac{1}{2} \\ 0 & \text{for } \left|\frac{\hat{t}}{T_P}\right| > \frac{1}{2} \end{cases} \tag{3}$$

and $\hat{t}$ is the fast time, t the full time, T_p the pulse width in seconds, f_0 the carrier frequency in Hz, and k the chirp rate.

The imaging geometry of a target with a jammer is shown in Fig. 2 where the coordinate XOY is established with the axis y is the light of sight (LOS). Suppose the translational motion has been
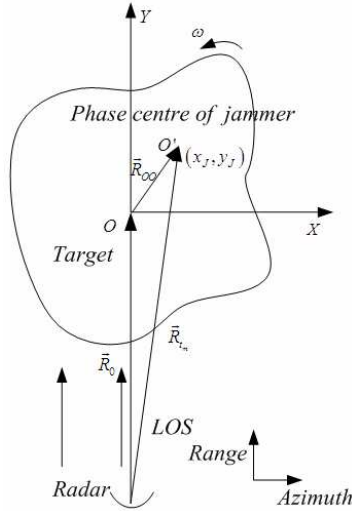
Figure 2. Geometry of ISAR imaging.

compensated and the target is a turntable model with angular velocity ω (rad/s) around the imaging centre O. $|\vec{R}_{t_m}|$ is the instantaneous slant range between O' (phase centre of the jammer) and radar. In a small accumulation angle $|\vec{R}_{t_m}|$ can be expressed as

$$\left|\vec{R}_{t_m}\right| = \left|\vec{R}_0\right| + y_J + x_J \omega t_m \tag{4}$$

where $O'(x_J, y_J)$ denotes the range between the jammer and the rotating centre, and t_m is the slow time satisfying that $t_m = t - \hat{t}$.

The delay time caused by $|\vec{R}_{t_m}|$ can be expressed as

$$\tau_m = \frac{2\left|\vec{R}_0\right|}{c} + \frac{2y_J}{c} + \frac{2x_J\omega}{c}t_m \tag{5}$$

where c is the speed of electromagnetic wave.

Denote the delay time of jammer by τ_r, then the delay time caused by retransmission and $|\vec{R}_{t_m}|$ can be computed as

$$
\begin{aligned}
\tau_s &= \tau_r + \tau + \tau_m \\
&= \tau_r + \tau + \frac{2\left|\vec{R}_0\right|}{c} + \frac{2y_J}{c} + \frac{2x_J\omega}{c}t_m \\
&= \tau_0 + \frac{2\left|\vec{R}_0\right|}{c} + \frac{2x_J\omega}{c}t_m
\end{aligned}
\tag{6}
$$

where $\tau_0 = \tau_r + \tau + \frac{2y_J}{c}$.

Take the radar transmitting signal's time as the starting time, and then the unit amplitude intermittent sampling jamming signals can be written as

$$
\begin{aligned}
s_{J1}\left(\hat{t}, t_m\right) &= p\left(t\right) \cdot s_0\left(\hat{t} - \tau_s, t_m\right) \\
&= \left[\operatorname{rect}\left(\frac{t}{\tau}\right) * \sum_{n=0}^{N-1} \delta\left(t - nT_s\right)\right] \cdot s_0\left(\hat{t} - \tau_s, t_m\right) \\
&= \left[\operatorname{rect}\left(\frac{t}{\tau}\right) * \sum_{n=0}^{N-1} \delta\left(t - nT_s\right)\right] \cdot e^{j2\pi\left(f_0(t-\tau_s)+\frac{1}{2}k\left(\hat{t}-\tau_s\right)^2\right)}
\end{aligned}
\tag{7}
$$

Integer values of a radar pulse after the intermittent sampling are generated as

$$N = \left\lceil \frac{T_p}{T_s} \right\rceil \tag{8}$$

where $N = \lceil x \rceil$ indicates the greatest integer no less than or equal to x. It is clear that the jamming signals are made up of N segment LFM signals, whose frequency modulation slope is k, pulse width is τ, and frequency modulation bandwidth is $B_J = k\tau$.

2.2. Micro-motion Modulation in the Slow Time

The m-D of a rotating scatterer in addition to the target's bulk movement is a sinusoidal FM signal [15]. Let the modulation micro-Doppler be

$$f_d = \frac{2}{\lambda}\omega x_d + \frac{2}{\lambda}\omega' r' \cos\left(\omega' t_m\right) \tag{9}$$

where λ denotes the wave length, x_d the modulation rotating centre away from the jammer along the X axis, r' the rotation radius, and ω' the rotation rate

$$
\begin{aligned}
s_{J2}(\hat{t}, t_m) &= \left[\text{rect}\left(\frac{t}{\tau}\right) * \sum_{n=0}^{N-1} \delta(t - nT_s)\right] \cdot e^{j2\pi\left(f_0(t-\tau_s)+\frac{1}{2}k(\hat{t}-\tau_s)^2\right)} \cdot e^{j2\pi \oint f_d t_m} \\
&= \left[\text{rect}\left(\frac{t}{\tau}\right) * \sum_{n=0}^{N-1} \delta(t - nT_s)\right] \cdot e^{j2\pi\left(f_0(t-\tau_s)+\frac{1}{2}k(\hat{t}-\tau_s)^2\right)} \\
&\quad \cdot e^{j\frac{4\pi}{\lambda}(\omega x_d t_m + r'\sin(\omega' t_m))}
\end{aligned}
\tag{10}
$$

Usually, ISAR targets are relatively small. For a wideband LFM signal, dechirping processing is an acceptable method to achieve a high resolution range profile (HRRP) [31]. Let the reference point be the imaging center O, then the jamming signals after dechirping can be expressed as

$$
\begin{aligned}
s_{J3}\left(\hat{t}, t_m\right) &= \left[\text{rect}\left(\frac{t}{\tau}\right) * \sum_{n=0}^{N-1} \delta\left(t - nT_s\right)\right] \cdot e^{-j2\pi k\left(\tau_0 + \frac{2x_J\omega}{c}t_m\right)\hat{t}} \\
&\quad \cdot e^{-j2\pi f_0\left(\tau_0 + \frac{2x_J\omega}{c}t_m\right)} \cdot e^{j\frac{4\pi}{\lambda}(\omega x_d t_m + r'\sin(\omega' t_m))}
\end{aligned}
\tag{11}
$$

2.3. ISAR imaging of the jamming signals

There are two steps of ISAR imaging: the range compression and the azimuth focusing. The jamming signals after the range compression in the fast-time domain are given by

$$
\begin{aligned}
s_{J4}(f_r, t_m) &= \sum_{n=-\infty}^{\infty} \tau f_s T_p \text{sinc}(nf_s\tau)\text{sinc}\left[T_p\left(f_r - nf_s - k\left(\tau_0 + \frac{2x_J\omega}{c}t_m\right)\right)\right] \\
&\quad \cdot e^{-j2\pi f_0\left(\tau_0 + \frac{2x_J\omega}{c}t_m\right)} \cdot e^{j\frac{4\pi}{\lambda}(\omega x_d t_m + r'\sin(\omega' t_m))}
\end{aligned}
\tag{12}
$$

where $\text{sinc}(x) \triangleq \frac{\sin(\pi x)}{\pi x}$. Suppose that no range migration occurs during the imaging time then the approximation form of (12) satisfies

$$
s_{J4}\left(f_r, t_m\right) = \sum_{n=-\infty}^{\infty} a_n \cdot e^{-\left[j\frac{4\pi}{\lambda}\omega(x_J - x_d)t_m - jZ\sin(\omega' t_m)\right]} \tag{13}
$$

where $a_n = \tau f_s T_p \mathrm{sinc}(n\tau f_s) \mathrm{sinc}[T_p(f_r - nf_s - k(\tau_0 + \frac{2x_J\omega}{c}t_m))]e^{-j2\pi f_0\tau_0}$ and $Z = \frac{4\pi}{\lambda}r'$.

Carrying out the FT in the slow-time domain, we can obtain the ISAR image [13, 15]

$$s_{J4}(f_r, f_a) = \sum_{n=-\infty}^{\infty} a_n \cdot \mathbb{F}\left\{e^{-\left[j\frac{4\pi}{\lambda}\omega(x_J-x_d)t_m - jZ\sin(\omega't_m)\right]}\right\}$$

$$= \sum_{n=-\infty}^{\infty} a_n \cdot \mathbb{F}\left\{\sum_{l=-\infty}^{\infty} J_l(Z)e^{-j\left[\frac{4\pi}{\lambda}\omega(x_J-x_d)-l\omega'\right]t_m}\right\}$$

$$= \sum_{n=-\infty}^{\infty} a_n T_M \cdot \left\{J_0(Z)\mathrm{sinc}\left[T_M\left(f_a - \frac{2}{\lambda}(x_J - x_d)\right)\right]\right.$$

$$+ J_1(Z)\mathrm{sinc}\left[T_M\left(f_a - \frac{2}{\lambda}(x_J - x_d) - \frac{\omega'}{2\pi}\right)\right]$$

$$- J_1(Z)\mathrm{sinc}\left[T_M\left(f_a - \frac{2}{\lambda}(x_J - x_d) + \frac{\omega'}{2\pi}\right)\right]$$

$$+ J_2(Z)\mathrm{sinc}\left[T_M\left(f_a - \frac{2}{\lambda}(x_J - x_d) - 2 \times \frac{\omega'}{2\pi}\right)\right]$$

$$\left. - J_2(Z)\sin c\left[T_M\left(f_a - \frac{2}{\lambda}(x_J - x_d) + 2 \times \frac{\omega'}{2\pi}\right) + \ldots\right]\right\} \quad l \in \mathbb{Z} \quad (14)$$

where T_M denotes the imaging time and $J_l(Z)$ the Bessel function of first kind.

From (14), one can conclude that the image of jamming signals is a series of scaled sinc functions in different bins, with its sidebands equally spaced at multiples of $\frac{\omega'}{2\pi}$ in the cross-range. In addition, the bandwidth of the m-D is about $2Z$, which is a function of wave length and rotation radius. Therefore, the jamming may contaminate the image of the main body in both the range and Doppler domain, particularly when it is emphatic.

3. TWO STEPS TO DETERMINE THE KEY PARAMETERS

Each sinc in (14) would be identified as a fake "point" target or a point-scatterer in radar, and according to the principle of time-frequency conversion, the distance in the down-range and the distance in the cross-range among scatterers are given by [31]

$$d_r = \frac{cf_s}{2k} \quad \text{and} \quad d_a = \frac{\lambda}{4\pi}\frac{\omega'}{\omega} \quad (15)$$

respectively.

For the sake of covering a target which takes up of $d_\parallel$ (down-range) $\times d_\perp$ (cross-range) m^2, there are two conditions that need to be met: a, the distance array (d_r, d_a) should not be too sparse; b, the available jamming area $\Delta_\parallel$ (down-range) $\times \Delta_\perp$ (cross-range) should be large enough. In order to satisfy the condition a, values of f_s and ω' should be chosen properly taking no account of the peak amplitude of each fake scatterer first [22, 29]. Usually, we need that

$$d_r \in (2 \sim 10)\,\sigma_r \quad \text{and} \quad d_a \in (2 \sim 10)\,\sigma_a \tag{16}$$

where $\sigma_r = \frac{c}{2B}$ and $\sigma_a = \frac{\lambda}{2\omega T_M}$ are the resolution in the down-range and cross-range. So it can be obtained that

$$f_s \in (2 \sim 10) \times \frac{1}{T_p} \quad \text{and} \quad \omega' = (2 \sim 10) \times \frac{2\pi}{T_M} \tag{17}$$

The next step is to fulfill condition b. As the available jamming area is determined by the down-range bins indexed by N and cross-range bins indexed by L, the amplitude of the fake scatterer indexed by (n, l) is

$$A(n, l) = \tau f_s T_p T_M \text{sinc}(n\tau f_s)\,J_l(Z) \tag{18}$$

Then condition b means that $A(n, l)$ should be no less than the amplitude of the scatterers of the target. The amplitude of the target echo is $T_p T_M$ as can be known from (14). So if the amplitude of a fake scatterer is equal to that of the true one, the amplitude ratio of the fake scatterer to the true one, namely the amplitude modulation coefficient, should be

$$M_J = \frac{T_p T_M}{\tau f_s T_p T_M \text{sinc}(n\tau f_s)\,J_l(Z)} = \frac{1}{\tau f_s \text{sinc}(n\tau f_s)\,J_l(Z)} \tag{19}$$

So condition b can be expressed by [31]

$$M_J^2 \le \frac{P_J}{P_T} \cdot \frac{4\pi\gamma R^2}{G\sigma} \tag{20}$$

with P_J denoting the jamming equivalent radiated power, G the radar antenna gain, P_T the radar peak power, σ the maximum radar cross section of the target, γ (usually supposed to be 0.5) the mismatch loss of polarizatio, and R the slant range.

The amplitude of $J_l(Z)$ and the spread of l along with Z are illustrated in Fig. 3. It is already known that $L \approx Z+1$ and $l \in (-L, L)$ for $Z \gg 1$ [33]. The cover area $\Delta_\perp$ equals $(2L+1) \times d_a$, and r' can be computed by

$$(2Z + 3) \times d_a \ge d_\perp \Rightarrow r' \ge \frac{\lambda}{8\pi}\left(\frac{d_\perp}{d_a} - 3\right) \tag{21}$$

(a) three-dimension graph

(b) planar graph
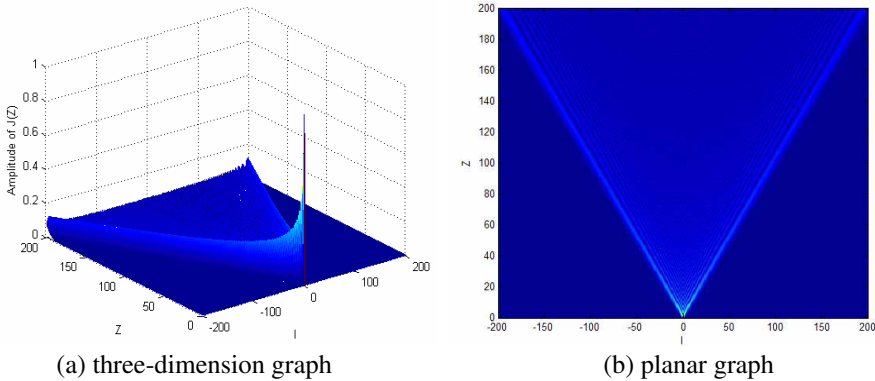
Figure 3. Graph of $J_l(Z)$ and l along with Z.
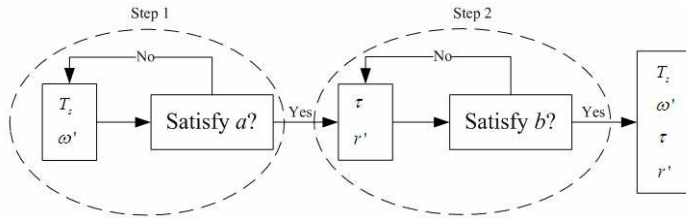
Figure 4. Flow chart to determine the jamming parameters.

Usually, r' will be very small referring to (21) for a radar in X band, and then $\Delta_\perp$ will be large enough to cover the ISAR imaging scene in cross-range. Then according (20), the value of τ can be decided at last. The flow chart of the parameter decision is shown in Fig. 4.

Generally, when P_J is enough, there will be many choices of τ maintaining (20). However, with the permission of realization, the smaller value of τ is, the more rapid response and more uniform of fake scatterers in amplitude will be generated [29]. Uniform amplitude of fake scatterers will generate a better contaminated ISAR image than that some nail-like peak value of amplitude near the imaging centre.

4. SIMULATIONS AND ANALYSIS

To further analyze the effect of the jamming, an ISAR imaging simulation of target with a jammer is presented in this part. The flow chart of the simulation is given in Fig. 5.

The main simulation parameters are listed in Table 1. The range

from the centre of the target and the radar is chosen as 40 km for the approximation of far-field backscattered field condition. The reference distance is also assumed to be 40 km which means that the target is rotating with its centre.

The target model with a finite number of perfect point scatterers

Table 1. Simulation parameters.

f_0	**10 GHz**	R	**40 km**	B	**300 MHz**	ω	**0.04π rad/s**
T_P	**100 μs**	σ	**0.1 m^2**	P_T	**1 kW**	T_M	**0.512 s**
PRF	**1000 Hz**	P_J	**10 w**	G	**30 dB**	γ	**0.5**

Radar transmitter	→	Target	→	Intermittent sampling	→	Micro-motion modulation	→	Radar receiver	→	Motion compensation	→	R-D Imaging
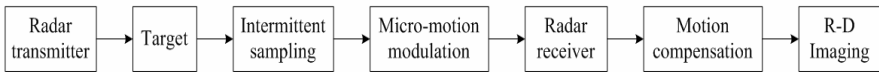
Figure 5. The flow chart of the numeric simulations.

(a)

(b)

(c)

(d)
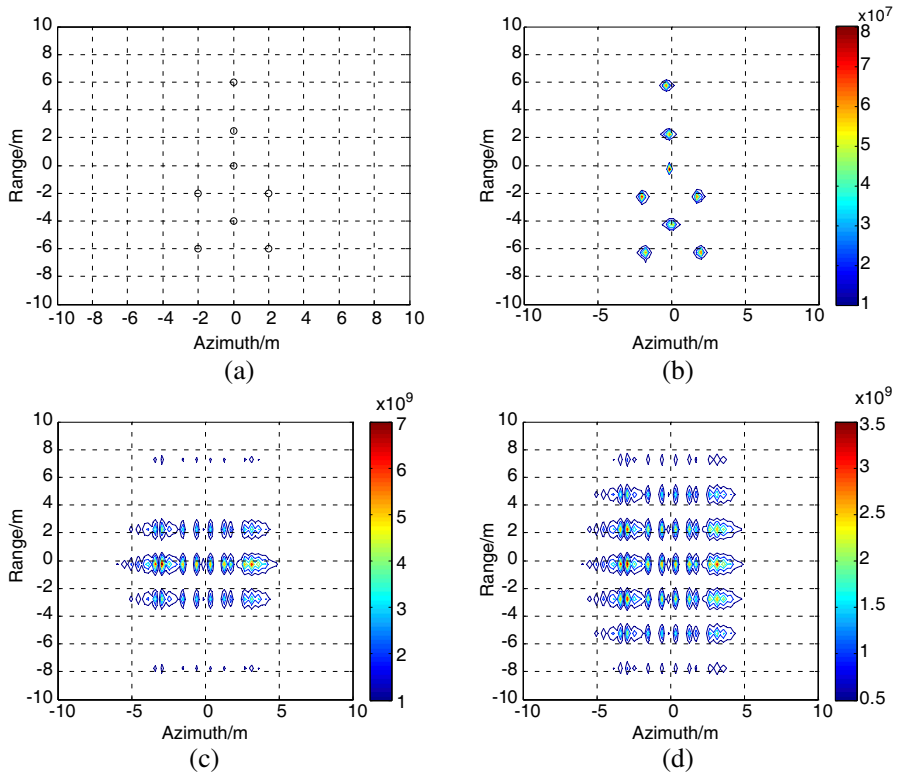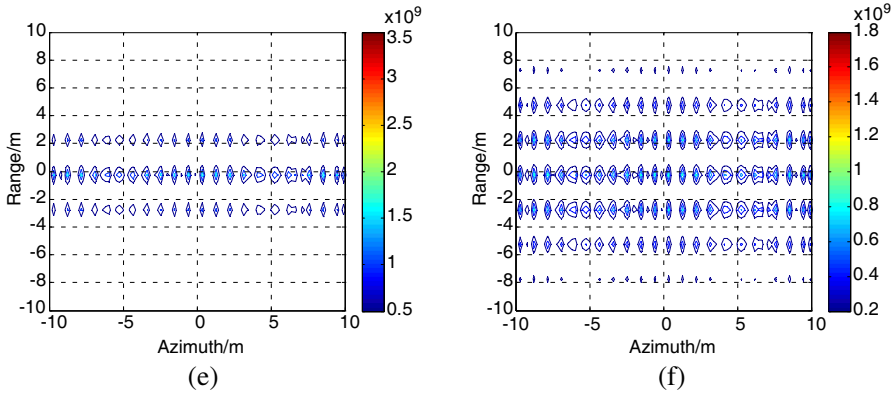
Figure 6. Images of the numeric simulation data. (a) Target model (point-scattering model). (b) Image without jamming. (c) Image with jamming ($r' = 0.02$ m, $\tau = 10$ μs). (d) Image with jamming ($r' = 0.02$ m, $\tau = 5$ μs). (e) Image with jamming ($r' = 0.2$ m, $\tau = 10$ μs). (f) Image with jamming ($r' = 0.2$ m, $\tau = 5$ μs).

is assumed to be located as shown in Fig. 6(a) and takes up 12×4 m^2, and the imaging center and the jammer are all located at $(0, 0)$. For the purpose of simplicity, the point scatterers are assumed to scatter the electromagnetic energy in all directions and in all angles with $\sigma = 0.1$ m^2 which is good enough for modeling as mentioned in [3]. Without loss of generality, this paper considers the imaging model of targets on the 2-D imaging plane.

According to (17), let $T_S = 20$ μs and $\omega' = 8\pi$ rad/s. r' should be no less than 0.02 m according to (21). We take four groups of parameters into the simulation: 1) $r' = 0.02$ m, $\tau = 10$ μs; 2) $r' = 0.02$ m, $\tau = 5$ μs; 3) $r' = 0.2$ m, $\tau = 10$ μs; 4) $r' = 0.2$ m, $\tau = 5$ μs.

ISAR imaging of the target without jamming is shown in Fig. 6(b). Comparing Figs. 6(c) and (d), Fig. 6(e) and Fig. 6(f), it can be seen that the target's image is all covered and smeared in these four figures, but more totally in Figs. 6(d) and (f) for the amplitude of fake scatterers are more uniform with a smaller τ ($= 5$ μs) as mentioned above. When $\omega' = 8\pi$ rad/s and $r' = 0.02$ m, we have that $Z \approx 8$ and $\Delta_\perp \approx 9$ m as shown in Fig. 6(c) and Fig. 6(d). If $r' = 0.2$ m, then we have $Z \approx 83$ and $\Delta_\perp \approx 79$ m as shown in Fig. 6(e) and Fig. 6(f) which has already exceeded the imaging scene in the cross-range. Comparing Fig. 6(c) and Fig. 6(e), Fig. 6(d) and Fig. 6(f), it can be figured out that $\Delta_\perp$ has been spread with the increment of r'. The strength of the scatterers in Fig. 6(e) and Fig. 6(f) indicated by the corresponding

colorbar is smaller than that in Fig. 6(c) and Fig. 6(d) as the increment of r'. On the other hand, when r' is the same, the strength of the scatterers reduces as the decrement of τ.

5. SIMULATIONS BASED ON MEASURED DATA

In this section, the jamming method is applied to the measured data of a real target. The measured data is obtained by a radar with the bandwidth of 400 MHz, pulse duration of 125 µs, and PRF of 400 Hz. The simulated jamming data is obtained based on the measured data. The flow chart of the jamming simulations based on the real data is illustrated in Fig. 7. From Fig. 5 and Fig. 7, it can be seen that the difference between the numeric simulations and the simulations based on measured data is that the intermittent sampling and the micro-motions modulation processing is after the radar receiver. According to the theory of the linear signal and system, the two simulations are equivalent in the flow.

As shown in Fig. 8(a), the real data are from a plane with 34.88-meter in wingspan and 36.8-meter in length. Take 256 echoes for ISAR imaging, then the coherent time $T_M = 0.64$ s. The ISAR image of the plane is illustrated in Fig. 8(b). Let $T_S = 25$ µs and $\omega' = 6\pi$ rad/s according to (17). r' should be no less than 0.06 m referring to (21). Take four groups of parameters into the experiments: 1) $r' = 0.06$ m, $\tau = 12.5$ µs; 2) $r' = 0.06$ m, $\tau = 5$ µs; 3) $r' = 0.2$ m, $\tau = 12.5$ µs; 4) $r' = 0.2$ m, $\tau = 5$ µs.

In experiments 1) and 2), when $r' = 0.06$ m, $\Delta_\perp$ is approaching 40 m as shown in Fig. 8(c) and Fig. 8(d). In experiments 3) and 4), when $r' = 0.2$ m, $\Delta_\perp$ equals 123 m as shown in Fig. 8(e) and Fig. 8(f) which has exceeded the imaging scene in the cross-range. The simulation results based on the measured data also illustrate that the strength of point-scatterers decreases with the increment of r' and decrement of τ which is similar to the results depicted in the numeric simulations.
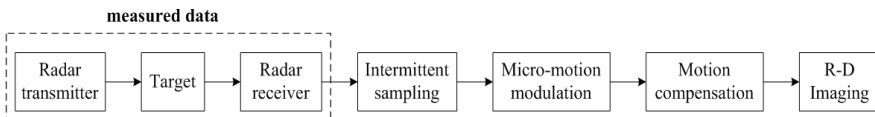
Figure 7. The flow chart of the jamming simulations based on measured data.
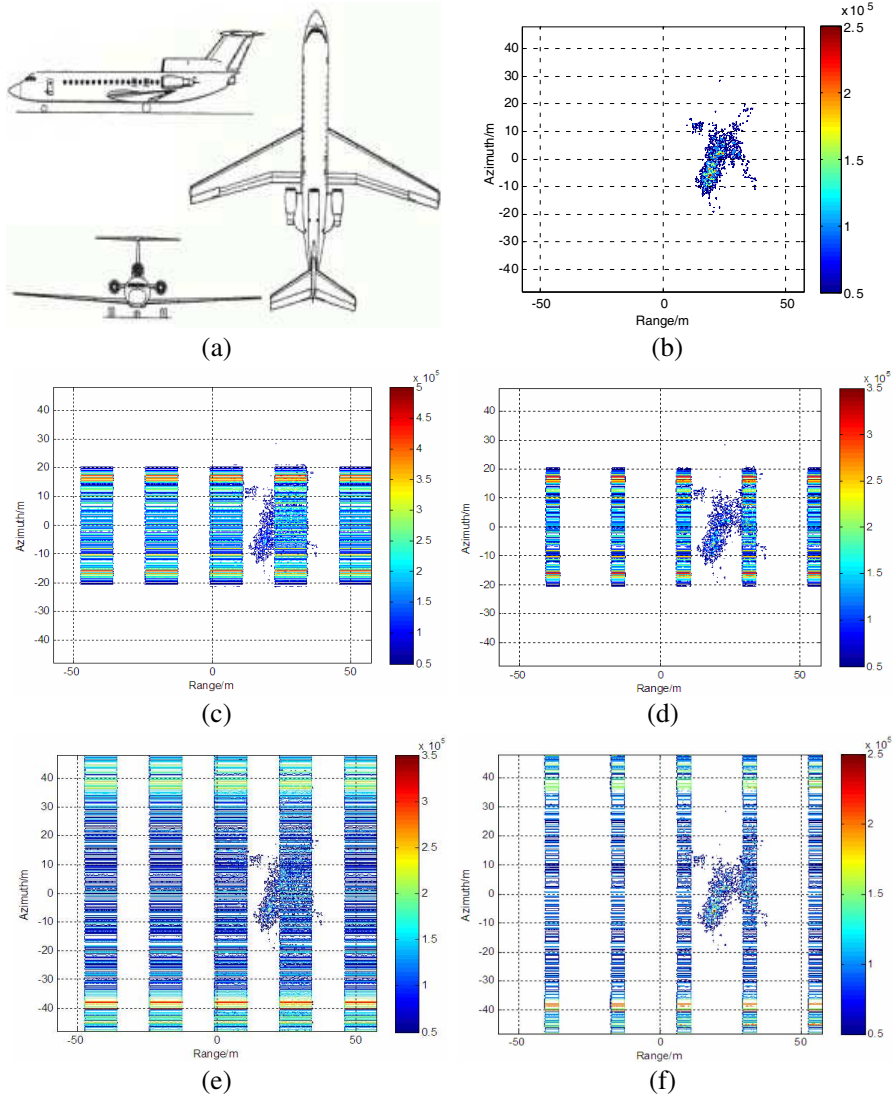
Figure 8. Images of the simulations based on measured data. (a) Framework for the plane. (b) Image without jamming. (c) Image with jamming ($r' = 0.06$ m, $\tau = 12.5\,\mu$s). (d) Image with jamming ($r' = 0.06$ m, $\tau = 5\,\mu$s). (e) Image with jamming ($r' = 0.2$ m, $\tau = 12.5\,\mu$s). (f) Image with jamming ($r' = 0.2$ m, $\tau = 5\,\mu$s).

6. CONCLUSIONS

This paper proposes a new ISAR countermeasure based on the ISRJ and micro-motion modulation. Numeric simulations are performed

to test the performance of the jamming. Furthermore, jamming experiments based on measured data are provided to validate the effectiveness of the jamming method. The results show that the proposed jamming method smears the ISAR image of a target in the RD imaging plane. One of the main challenges of this jamming method is that the jamming energy actually spreads out into the 2-D intensity image. The selection criteria of jamming parameters is important. The essential requirement for the jamming energy will be addressed in the further work.

REFERENCES

1. Chen, C. C. and H. C. Andrews, "Target-motion-induced radar imaging," *IEEE Transactions on Aerospace and Electronic Systems*, Vol. 16, 2–14, 1980.

2. Ausherman, D. A., A. Kozma, J. L. Walker, H. M. Jones, and E. C. Poggio, "Developments in radar imaging," *IEEE Transactions on Aerospace and Electronic Systems*, Vol. 20, 363–400, 1984.

3. Chen, V. C. and W. J. Miceli, "Simulation of ISAR imaging of moving targets," *IEE Proceedings Radar, Sonar and Navigation*, Vol. 148, 160–166, 2001.

4. Berizzi, E., "ISAR imaging of targets at low elevation angles," *IEEE Transactions on Aerospace and Electronic Systems*, Vol. 31, 419–435, 2001.

5. Avent, R. K., J. D. Shelton, and P. Brown, "The ALCOR C-band imaging radar," *IEEE Antennas and Propagation Magazine*, Vol. 38, 16–17, 1996.

6. Pace, P. E., D. J. Fouts, S. Ekestorm, and C. Karow, "Digital false-target image synthesiser for countering ISAR," *IEE Proc. — Radar Sonar Navig.*, Vol. 149, 248–257, 2002.

7. Delaney, W. P. and W. W. Ward, "MIT Lincoln laboratory journal: Fifty years of radar," *IEEE Aerospace and Electronic Systems Magazine*, Vol. 18, 37–38, 2003.

8. Schuerger, J. and D. Garmatyuk, "Deception jamming modeling in radar sensor networks," *Proceedings of IEEE Military Communications Conference (MILCOM'08)*, 1–7, Washington, DC, USA, 2008.

9. Xu, S. K., J. H. Liu, Y. W. Fu, and X. Li, "Deception jamming method for ISAR based on sub-Nyquist sampling technology," *ICSP'2010 Proceedings*, 2023–2026, 2010.

10. Li, J. and H. Ling, "Application of adaptive chirplet representa-

tion for ISAR feature extraction from targets with rotating parts,"
IEE Proceedings Online, Vol. 150, No. 20030729, 284–291, 2003.

11. Li, X., B. Deng, Y. L. Qin, H. Q. Wang, and Y. P. Li, "The
influence of target micromotion on SAR and GMTI," *IEEE
Transactions on Aerospace and Electronic Systems*, Vol. 49, 2738–
2751, 2011.

12. Li, K. M., X. J. Liang, Q. Zhang, Y. Luo, and H. J. Li, "Micro-
doppler signature extraction and ISAR imaging for target with
micromotion dynamics," *IEEE Geoscience and Remote Sensing
Letters*, Vol. 8, 411–415, 2011.

13. Chen, V. C., F. Li, S. S. Ho, and H. Wechsler, "Micro-doppler
effect in radar-phenomenon, model, and simulation study," *IEEE
Transactions on Aerospace and Electronic Systems*, Vol. 24, 1–21,
2006.

14. Li, G., H. Zhang, and X. Q. Wang, "ISAR 2-D imaging
of uniformly rotating targets via matching pursuit," *IEEE
Transactions on Aerospace and Electronic Systems*, Vol. 48, 1838–
1846, 2012.

15. Bai, X. R., M. D. Xing, F. Zhou, G. Y. Lu, and Z. Bao, "Imaging of
micromotion targets with rotating parts based on empirical-mode
decomposition," *IEEE Transactions on Aerospace and Electronic
Systems*, Vol. 46, 3514–3523, 2008.

16. Bai, X. R., F. Zhou, M. D. Xing, and Z. Bao, "High resolution
ISAR imaging of targets with rotating parts," *IEEE Transactions
on Aerospace and Electronic Systems*, Vol. 47, 2530–2543, 2011.

17. Chen, V. C., "Doppler signatures of radar backscattering from
objects with micro-motions," *IET Signal Process.*, Vol. 2, 291–
300, 2008.

18. Thayaparan, T., G. Lampropoulos, S. K. Wong, and E. Rise-
borough, "Application of adaptive joint time-frequency algorithm
for focusing distorted ISAR images from simulated and measured
radar data," *IEE Proc. — Radar Sonar Navig.*, 213–220, 2003.

19. Ljubiša, S., D. Igor, and T. Thayaparan, "Separation of target
rigid body and micro-doppler effects in ISAR imaging," *IEEE
Transactions on Aerospace and Electronic Systems*, Vol. 42, 1496–
1506, 2006.

20. Zhang, Q., T. S. Yeo, H. S. Tan, and Y. Luo, "Imaging of a moving
target with rotating parts based on the hough transform," *IEEE
Transactions on Aerospace and Electronic Systems*, Vol. 46, 291–
299, 2008.

21. Luo, Y., Q. Zhang, C. W. Qiu, X. J. Liang, and K. M. Li, "Micro-

doppler effect analysis and feature extraction in ISAR imaging with stepped-frequency chirp signals," *IEEE Transactions on Aerospace and Electronic Systems*, Vol. 48, 2087–2098, 2010.

22. Bai, X. R., G. C. Sun, F. Zhou, M. D. Xing, and Z. Bao, "A novel ISAR jamming method based on rotating angular reflector," *Chinese Journal of Radio Science*, Vol. 23, 867–872, 2008.

23. Adler, E. and E. Viverios, *Direct Digital Synthesis Application for Radar Development*, Washington, DC, 1995.

24. Berger, S. D., "Digital radio frequency memory linear range gate stealer spectrum," *IEEE Transactions on Aerospace and Electronic Systems*, Vol. 39, 725–735, 2003.

25. Zhang, Y., C. X. Dong, Y. P. Cui, and S. Q. Yang, "Coherent jamming technique countering ISAR," *Acta Electronica Sinica*, Vol. 34, 1590–1595, 2006.

26. Liu, Q., S. Xing, X. Wang, J. Dong, D. Dai, and Y. Li, "The 'Slope' effect of coherent transponder in InSAR DEM," *Progress In Electromagnetics Research*, Vol. 127, 351–370, 2012.

27. Zhu, B. Y., L. Xue, and D. P. Bi, "A micro-motion feature deception jamming method to ISAR," *ICSP'2010 Proceedings*, 2287–2290, 2010.

28. Zhu, B. Y., L. Xue, and D. P. Bi, "A novel method of ISAR jamming based on synthesizing equivalent micro-motion point," *Modern Radar*, Vol. 33, 33–36, 2011.

29. Feng, D. J., H. M. Tao, Y. Yang, and Z. Liu, "Jamming de-chirping radar using interrupted-sampling repeater," *Science China: Information Sciences*, Vol. 54, 2138–2146, 2011.

30. Wang, X. S., J. C. Liu, W. M. Zhang, Q. X. Fu, Z. Liu, and X. X. Xie, "Mathematic principles of interrupted-sampling repeater jamming (ISRJ)," *Science in China, Series F: Information Sciences*, Vol. 50, 113–123, 2007.

31. Caputi, W. J., "Stretch: A time-transformation technique," *IEEE Transactions on Aerospace and Electronic Systems*, Vol. 7, 269–278, 1971.

32. Schleher, D. C., *Electronic Warfare in the Information Age*, Artech House, London, 1999.

33. Gini, F. and G. B. Giannakis, "Hybrid FM-polynomial phase signal modeling: Parameter estimation and Cramer-Rao bounds," *IEEE Transactions on Signal Processing*, Vol. 47, 363–377, 1994.